Developmental Biology 372 (2012) 55–67

Contents lists available at SciVerse ScienceDirect

Developmental Biology

journal homepage: www.elsevier.com/locate/developmentalbiology

In vivo knockdown of Brachyury results in skeletal defects and urorectal malformations resembling caudal regression syndrome ☆

Tracie Pennimpede [a], Judith Proske [a], Andrea König [a], Joana A. Vidigal [a,1], Markus Morkel [a,c], Jesper B. Bramsen [a,2], Bernhard G. Herrmann [a,b], Lars Wittler [a,*]

[a] Max Planck Institute for Molecular Genetics, Developmental Genetics Department, Ihnestraße 73, 14195 Berlin, Germany
[b] Charité University Medicine Berlin, Institute for Medical Genetics, Campus Benjamin Franklin, Hindenburgdamm 30, 12203 Berlin, Germany
[c] Charité University Medicine Berlin, Institute for Pathology, Charitéplatz 1, 10117 Berlin, Germany

ARTICLE INFO

Article history:
Received 15 December 2011
Received in revised form
20 August 2012
Accepted 7 September 2012
Available online 18 September 2012

Keywords:
Brachyury
RNAi knockdown
Hypomorph
Notochord
Murine development
Axial development
Urorectal malformations
Mesoderm survival
Caudal regression

ABSTRACT

The T-box transcription factor BRACHYURY (T) is a key regulator of mesoderm formation during early development. Complete loss of *T* has been shown to lead to embryonic lethality around E10.0. Here we characterize an inducible miRNA-based *in vivo* knockdown mouse model of *T*, termed *KD3-T*, which exhibits a hypomorphic phenotype. *KD3-T* embryos display axial skeletal defects caused by apoptosis of paraxial mesoderm, which is accompanied by urorectal malformations resembling the murine uro-recto-caudal syndrome and human caudal regression syndrome phenotypes. We show that there is a reduction of T in the notochord of *KD3-T* embryos which results in impaired notochord differentiation and its subsequent loss, whereas levels of T in the tailbud are sufficient for axis extension and patterning. Furthermore, the notochord in *KD3-T* embryos adopts a neural character and loses its ability to act as a signaling center. Since *KD3-T* animals survive until birth, they are useful for examining later roles for T in the development of urorectal tissues.

Introduction

Brachyury (literally 'short tail') is a semi-dominant mutation which was first described in 1927 from the phenotypic analysis of a spontaneously occurring mouse mutant (Dobrovolskaïa-Zavadskaïa, 1927). Cloning of the *Brachyury* gene, termed *T,* established that it codes for a transcription factor, which was the first T-box gene to be molecularly characterized (Herrmann et al., 1990; Kispert and Hermann, 1993). The *T* mutant has been verified to represent a true null, wherein the coding sequence is entirely absent (Herrmann et al., 1990).

During mouse gastrulation, *T* is expressed in nascent mesoderm at the primitive streak, and is downregulated in cells that leave the streak, *i.e.*, in paraxial and lateral plate mesoderm (Wilkinson et al., 1990). Expression persists in the mesoderm/primitive streak of the tailbud from early organogenesis stages until approximately embryonic day (E)12.5–E13.0. A second expression domain of *T* is found within the notochord, a transient rod-shaped structure located along the dorsal midline. Notochord precursor cells arise together with the definitive gut endoderm from the node (Sulik et al., 1994). During further development, the notochord precursor separates from the gut to form the mature notochord, and between E12.5 and E15.5 it becomes incorporated into the mucosa of the intervertebral discs. Notochordal *T* expression can be detected as soon as the notochord and its precursors are formed (*circa* E7.5) (Herrmann, 1991), and expression is maintained later in the intervertebral nuclei pulposi (Wilkinson et al., 1990). After tail formation and axial specification have ceased, transcripts of *T* are specifically confined to the notochord and its derivatives (Wilkinson et al., 1990).

Heterozygous $T^{+/-}$ mice exhibit a variably shortened tail, whereas homozygous $T^{-/-}$ mice die between E9.5 and E10.5. $T^{-/-}$ embryos display an overall loss of mesoderm caused by failure of epiblast cells to ingress through the primitive streak. Consequently, embryos have impaired axial development and allantoic defects, the latter of which are thought to be the cause of death (Gluecksohn-Schoenheimer, 1938, 1944; Yanagisawa,

☆ Grant Information: German Federal Ministry of Education and Research (BMBF) Federal Funding Program for Rare Diseases; Grant number 01GM08107.
* Corresponding author. Fax: +49 30 8413 1229.
E-mail address: wittler@molgen.mpg.de (L. Wittler).
[1] Current address: Department of Cancer Biology and Genetics, Memorial Sloan-Kettering Cancer Center, 1275 York Avenue, New York, NY 10065, USA.
[2] Current address: Department of Molecular Biology, Aarhus University, C.F. Møllers Allé, Build 1130, Aarhus C 8000, Denmark.

0012-1606/$ - see front matter © 2012 Elsevier Inc. All rights reserved.
http://dx.doi.org/10.1016/j.ydbio.2012.09.003

1990). $T^{-/-}$ embryos also display a kinked neural tube accompanied by disrupted somite formation (Chesley, 1935; Fujimoto and Yanagisawa, 1983; Gruneberg, 1958; Yanagisawa et al., 1981). Analysis of various *T* mutant alleles has illustrated that the severity of axis truncation directly correlates with gene dosage (Yanagisawa, 1990), and rescue of the tail length by complementation with a wildtype *T* transgene has confirmed this correlation (Stott et al., 1993). Since the anterior part of the embryo can be formed in the absence of *T*, it has been suggested that there is a greater requirement for *T* in posterior notochord development and caudal axis extension as development proceeds (Rashbass et al., 1991).

Development of the axial notochord and differentiation of paraxial somites are intimately linked processes. Mechanical and genetic manipulations have shown that regional specification of somites depends on secreted factors from the notochord and neural tube (Chiang et al., 1996; Dietrich et al., 1997; Pourquie et al., 1993; Teillet et al., 1998; Teillet and Le Douarin, 1983). Both the notochord and the floor plate produce the morphogen Shh, and its expression in the notochord is essential for induction of the floor plate (Roelink et al., 1994), however, once the floor plate of the neural tube has been established, the notochord is no longer required for vertebral development (Ando et al., 2011). It has recently been shown that Shh is dispensable for vertebral formation after the notochord sheath appears (at approximately E10.0), which is a structure that surrounds the notochord cells, acting as a "wrapper" (Choi and Harfe, 2011). The notochord is absent in the caudal-most region of nearly all *T* mutants (Gruneberg, 1958; Yanagisawa, 1990), and the level of notochord loss has been found to correspond to the resulting length of the tail. Thus, the question arises as to whether the failure to maintain somites, and the observed caudal truncations, appear as a secondary effect due to loss of *T* in the notochord, decreased expression in the streak and tailbud mesoderm, or both.

We previously generated a series of transgenic knockdown animals for *Brachyury* using an *in vivo* miRNA strategy (Vidigal et al., 2010). This work describes the in-depth analysis of one of the knockdown lines from this work (*KD3-T*), wherein embryos exhibit a phenotype for *Brachyury* which is intermediate to the heterozygous and homozygous-null states. We show that this phenotype results primarily from an early and sustained knockdown of *T* in the notochord which does not allow for differentiation of a mature notochord structure. We further show that this reduction in functional T results in death of paraxial mesoderm cells posterior to the hindlimb, which culminates in axial and urorectal defects. Notably, the highly reproducible association of skeletal defects, malformations in urorectal tissues, and spina bifida in induced *KD3-T* embryos phenocopy the hallmarks of human Caudal Regression Syndrome (Sacral Defect with Anterior Meningocele; OMIM #600145) and thus may provide a useful model for studying the causes and progression of this congenital disorder.

Results and discussion

Generation of a phenotypically hypomorphic T mutant by in vivo knockdown of Brachyury

We have recently established a Cre recombinase-mediated cassette exchange (RMCE) system for the robust *in vivo* knockdown of genes in the developing mouse embryo. This system utilizes shRNAmirs integrated into the *Gt(ROSA)26Sor* locus under control of a tetracycline-dependent transcriptional silencer (tTS) or reverse tetracycline-dependent transcriptional activator. Using this system we developed several knockdown models for *T* which exhibited varying phenotypic severities (Vidigal et al., 2010). One particular line from this transgenic series, $Gt(ROSA)26Sor^{tm3(tetO-EGFP,-RNAi:T)Bgh}$ (MGI:5297100), or *KD3-T*, was generated using a tTS-controlled transgene expressing a single shRNAmir against *T*, which was integrated into an intron after the coding sequence for EGFP (Fig. 1A). In this context the tTS is expressed ubiquitously from the *ROSA*26 promoter and is able to repress expression of the RNAi by binding to the tet-responsive element until repression is relieved upon treatment with doxycycline (Dox). Upon Dox treatment, the *KD3-T* transgene was expressed ubiquitously, as determined by monitoring EGFP expression (see Vidigal et al., 2010 and Fig. 4). In the experiments described here, the transgene was induced by Dox administration in the drinking water of the mother as soon as a vaginal plug was detected (at E0.5) and treatment was maintained until embryos were harvested for analysis. Since optimal knockdown by the miRNA is achieved within 24 h of Dox treatment (Vidigal et al., 2010), maximal knockdown of *T* via this transgene will persist throughout all stages of embryonic development.

KD3-T was found to display a milder phenotype than that observed upon total loss of *T* but stronger than $T^{+/-}$ (Chesley, 1935; Herrmann, 1991; Vidigal et al., 2010). Initially, we examined the gross morphological and histological attributes of the *KD3-T* embryos throughout development and observed that embryos exhibit functional notochord arrest near the forelimb level at E9.5–E10.5, as monitored by expression of *Shh*, but have a normal number of somites (Vidigal et al., 2010 and data not shown). Caudal defects are apparent by E10.5, and are characterized by a kinked neural tube located at a level between the fore and hindlimb buds. Between E10.5 and E11.5 the tail evolved into a rudiment, and by E12.5–E13.5 a wide but covered opening in the caudal neural tube could often be seen at the sacral level. Although death and/or resorption of induced *KD3-T* embryos was negligible before E12.5, the mortality of induced transgenic embryos increased as development proceeded, with only 35% transgenic embryos surviving past E13.5 (21 recovered/62 analyzed). The most striking reduction in transgenic animals recovered occurred between E14.5 and E15.5. The main cause of death in *T* null embryos is allantoic defects, and in our experiments such defects were occasionally noted in induced *KD3-T* embryos (Vidigal et al., 2010 and this work). Since the increased mortality in *KD3-T* embryos is seen after E13.5, it is possible that defects in branching at the chorioallantoic interface, which is known to require Bmp and Wnt signaling (Monkley et al., 1996; Watson and Cross, 2005; Ying and Zhao, 2001), could contribute to the observed increase in death at mid-to-late gestation. The few *KD3-T* embryos that survived until birth exhibited a tail filament and spina bifida, and died within a few hours due to apparent respiratory distress. Since the axial skeletal phenotype and resulting disorganization of internal caudal structures in surviving embryos at later stages was found to be quite variable, it is plausible that survival of *KD3-T* embryos is dependent on the severity of these defects, with more rostral levels of tissue disorganization and vertebral loss resulting in breathing difficulties due to ribcage malformations and lack of trunk musculature. This is consistent with defects seen in caudal regression syndrome, where failure-to-thrive is correlated with more anterior vertebral defects, and patients often exhibit compromised respiration (Boulas, 2009).

When we examined *T* expression in induced *KD3-T* embryos between E8.5 and E11.5 by whole-mount *in situ* hybridization (WISH), we observed that *T* could be detected in the tailbud at all stages examined (Fig. 1B). However, although *T* was initially present in some fragmented notochord cells at E8.5, it was absent from the node and notochordal plate, and could no longer be detected within the notochord at any axial level from E9.5

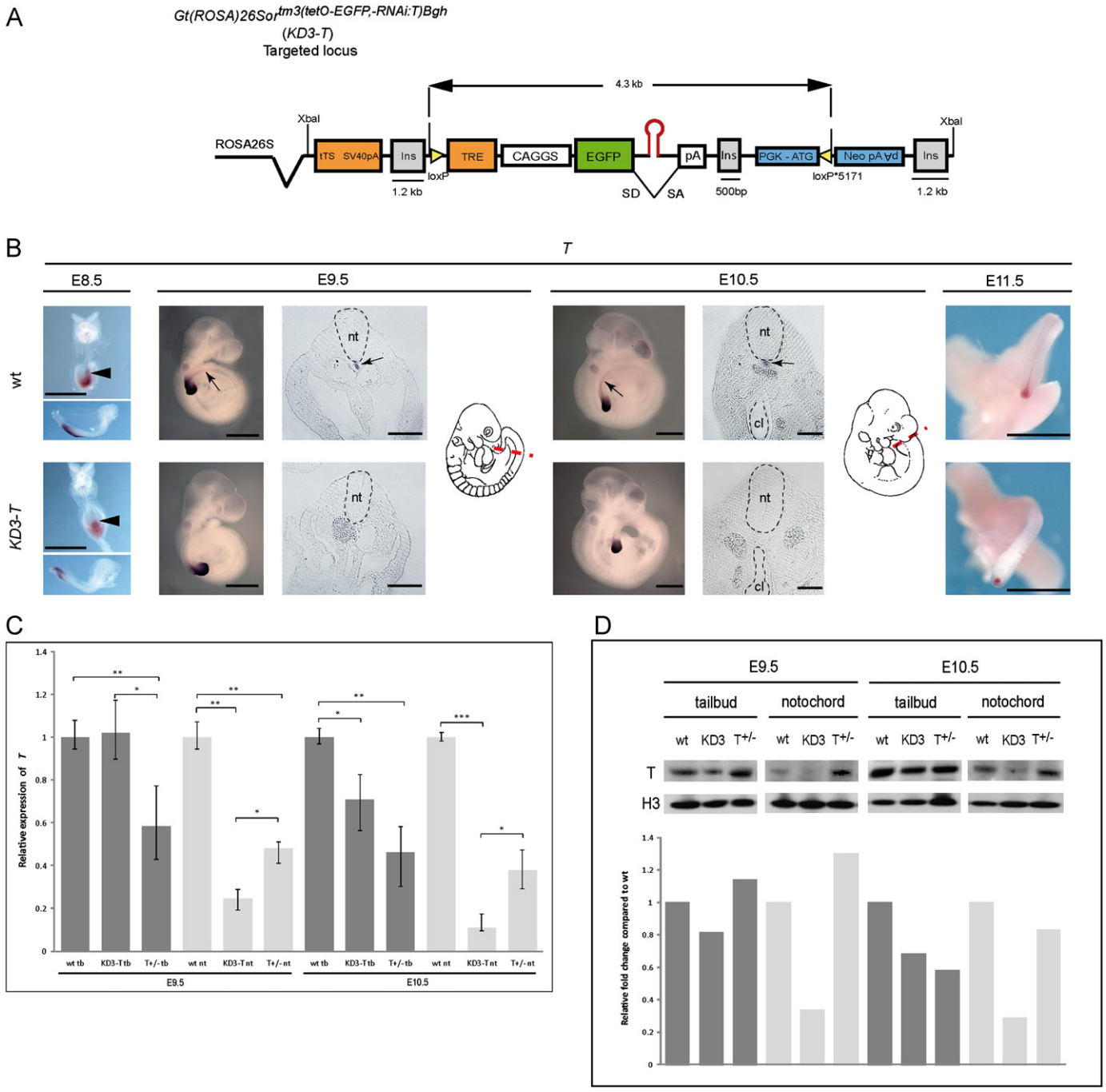

Fig. 1. *In vivo* knockdown of *Brachyury* using an intronic shRNA hairpin transcribed under control of a tet-responsive silencer results in efficient reduction of T in the notochord. (A) Schematic representation of the targeted locus containing the *Brachyury* knockdown transgene within intron one of *Gt(ROSA)26Sor*. The shRNA hairpin (red) is based on miR155 and was placed in the intron following the coding sequence for EGFP. See (Vidigal et al., 2010) for details. (B) WISH of transgenic embryos (*KD3-T*) along with wild type littermates (wt) from E8.5 to E11.5. *T* transcripts are undetectable in the notochordal plate and notochord of *KD3-T* embryos, whereas expression of *T* persists in the streak and presomitic mesoderm. Arrows point to expression of *T* in the notochord of wt embryos, and arrowheads indicate the node-associated notochordal plate at E8.5. Embryo drawings illustrate the level of the vibratome sections to the left, where the neural tube (nt, E9.5 and E10.5) and cloaca (cl, E10.5) are outlined by dotted lines. (C) Quantitative PCR analysis for *T* in tailbud and notochord samples isolated from wt, *KD3-T*, and $T^{+/-}$ embryos at E9.5 and E10.5. Levels of *T* were normalized to *Pmm2* and results are shown as fold-change relative to wild-type. Error bars represent standard deviation from the mean and statistical significance was determined using a student's paired *t*-test (* represents $p < 0.05$, ** is $p < 0.01$, and *** is $p < 0.001$). (D) Immunoblot for T and histone H3 (loading control) in tailbud and notochord samples isolated from wt, *KD3-T*, and $T^{+/-}$ embryos at E9.5 and E10.5, with densitometry levels shown below. Scale bars in B represent 0.5 mm for whole mounts and 0.1 mm for sections. CAGGS, CAGGS promoter; EGFP, enhanced green fluorescence protein coding region; Ins, chicken globin insulator; loxP/loxP*5171, sites for RMCE; Neo, neomycin resistance cassette; pA, polyA terminator; PGK, phosphoglycerate kinase promoter; SA/SD, splice donor and splice acceptor sites; TRE, tetracycline response element; tTS, tetracycline-dependent transcriptional silencer. (For interpretation of the references to color in this figure legend, the reader is referred to the web version of this article.)

(Fig. 1B). Quantification of *T* mRNA levels was performed by qPCR on dissected tailbud and more anterior notochord samples in *KD3-T* embryos at E9.5 and E10.5, as compared to wild-type littermates and $T^{+/-}$ embryos with the same outcrossed genetic background (Fig. 1C). As expected, *T* mRNA in heterozygotes was approximately 50% of wild-type levels in both the tailbud and

notochord samples at both stages examined, whereas the level of *T* in *KD3-T* tailbud was unchanged at E9.5 and significantly reduced to 70% at E10.5. Levels of *T* in the notochord were found to be significantly reduced at both E9.5 and E10.5 to 25% and 10% of wild-type levels, respectively. Immunoblotting for T confirmed that protein levels were greatly reduced in the *KD3-T* notochord at both stages, whereas the tailbud sample had a similar amount of T at E9.5, but showed a reduction at E10.5 (Fig. 1D). The levels of T protein in $T^{+/-}$ embryos at E10.5 mirrored what was seen at the mRNA level, while there was compensation at the protein level in the E9.5 $T^{+/-}$ tailbud and notochord samples. This may reflect a threshold requirement for *T* in generating feed-forward regulation of the protein at this stage. Although we cannot formally exclude that the reduction of T observed in the tailbud of *KD3-T* embryos contributes to the observed phenotype, overall these data strongly suggest that the *KD3-T* phenotype results mainly from loss of T in the notochord, since levels in the tailbud were similar to those in $T^{+/-}$ embryos, and *Brachyury* heterozygous mice in this genetic background exhibit only a variably shortened tail and never display urorectal defects.

Loss of BRACHYURY function in the notochord results in failure of the notochord to differentiate and maintain caudal structures

We next performed a histological examination of transverse sections of E10.5 embryos at the level of the hindlimb and cloaca. At this level and stage the notochord cells should be organized into a mature differentiated notochord structure. Morphological examination revealed that the notochord structure in *KD3-T* embryos was undifferentiated. Instead of exhibiting a compact morphology at this axial level and stage, the *KD3-T* notochord appeared larger and more tubular in structure, resembling the structure of a more caudal, less-differentiated notochord (Fig. 2A–D). Immunofluorescence detection of T and the neural marker Sox2 just below the level of the hindlimb confirmed that T was missing in this undifferentiated notochord structure, and that the notochord had instead adopted a neural character (Fig. 2E and F). This structure was also found to have low-to-undetectable levels of *Shh* expression, whereas *Shh* expression was maintained in the endodermal cloaca and the zone of polarizing activity (ZPA) of the limb buds (Fig. 2G–J). Moreover, *KD3-T* embryos showed a severe reduction in paraxial mesenchyme in the area surrounding the notochord, located between the cloaca and neural tube (Fig. 2A and C, brackets). Overall, this data illustrates that the remaining T protein present following knockdown in the *KD3-T* line is not sufficient to support notochord differentiation, and results in a loss of mesodermal character at the expense of neural character. This causes inability of the notochord to express *Shh* and act as a signaling center.

Histological analysis at E12.5 revealed that *KD3-T* embryos develop severe caudal defects posterior to the hindlimb, including disrupted somites (Fig. 2O). Failure to maintain the mesodermal fate of the notochord, and the resultant loss of the somites manifested in the appearance of unstructured dorsal tissue in the sacral region at the base of the tail. The size and appearance of the hindlimbs and the genital tubercle were found to be normal (Fig. 2K–R). Moreover, transverse sections at the level of the hindlimb showed that there was no detectable notochord or related structure at this stage (Fig. 2N and R), illustrating that the undifferentiated notochord structure observed at E10.5 degenerates by E12.5. Similar to what was observed at E10.5, at E12.5 we found *Shh* to be expressed normally in tissues located distant to the notochord, such as the urethral and rectal epithelia (ue and re; Fig. 2T and V), but absent from the notochord and floor plate (Fig. 2T asterisk and fp, compare with Fig. 2V). Lack of Shh signaling in the dorsal embryo was verified by an absence in the expression of its downstream target *Foxf1a* which was detected in the mesoderm of the genital tubercle, but not within the sclerotome (Fig. 2W–Z, s/s*).

The *KD3-T* phenotype is consistent with that expected upon loss of Hh signaling in the notochord. Removal of hedgehog signaling in the notochord via conditional deletion of *Smo*, or by deletion of *Shh* itself in the notochord, has been shown to cause increased cell death in somites posterior to the lumbar level at E12.5 (Choi and Harfe, 2011; Seifert et al., 2009). This is accompanied by reduced cell proliferation, and aberrant migration of notochord cells. Notably, embryos with targeted loss of notochord *Shh* expression or signaling have a tail filament similar to the one observed here (see Choi and Harfe, 2011; Seifert et al., 2009). Although, it has not been published whether the trunk mesoderm dorsal to the cloaca is affected in these mutants, it is likely to be the case since this region shows activated Hh signaling at E10.5 (Haraguchi et al., 2007).

Notochord cells are formed but unable to differentiate under conditions of low BRACHYURY

In order to refine the timing of notochord disruption, and further define the molecular cause of the defects seen in *KD3-T* embryos, we analyzed the expression of genes known to be essential for proper notochord and tailbud development by WISH. The expression of *Noto* is mainly confined to notochordal precursors, *i.e.*, it is expressed initially in the node and later in the caudal-most part of the notochord. Loss of *Noto* has been shown to result in variably penetrant caudal truncations confined to the tail and sacral region of the vertebral column, and *Noto* expression was previously found to be absent in $T^{-/-}$ embryos (Abdelkhalek et al., 2004). At E9.5 and E10.5 expression of *Noto* could be detected in the caudal notochord of both wild-type and *KD3-T* embryos (Fig. 3A–D), illustrating that notochord precursor cells are present and able to form a nascent notochord structure in *KD3-T* embryos.

The tailbud is a signaling center important for axial elaboration of the embryo. In order to analyze whether the reduction of T observed at the mRNA and protein levels in the tailbud of *KD3-T* embryos (see Fig. 1C and D) contributes functionally to caudal malformations in *KD3-T* mice, we examined the expression of genes in the tailbud including *Cyp26a1* (Fig. 3E–H), along with *Hoxd13* and *Sall3* (see Fig. 7). The gene for *Cyp26a1* encodes a RA catabolic enzyme which is strongly expressed in tailbud mesoderm (MacLean et al., 2001), and loss of this gene causes severe caudal regression (Abu-Abed et al., 2001; Sakai et al., 2001). Misregulation of *Cyp26a1* was found in another of the transgenic models that we had previously generated, which exhibits strong knockdown of *T* in both the notochord and the tailbud (*KD1-T*, see Vidigal et al., 2010). However, at E9.5 and E10.5, *Cyp26a1* was found to be present in tailbuds of both the *KD3-T* embryos and their wild-type littermates. Expression of both *Hoxd13* and *Sall3* was also maintained in the caudal region of *KD3-T* embryos at E10.5 and later (Fig. 7A and B), verifying that primary axis extension proceeded normally. Taken together, the expression data illustrate that T is present at functionally sufficient amounts in the tailbud but not the notochord of *KD3-T* embryos. These levels are able to maintain early embryonic development along the rostrocaudal axis and formation of notochord precursor cells, but not the mesodermal fate of the notochord structure. This is in contrast to the effect of loss of *T* in both the notochord and the tailbud mesoderm, which leads to complete caudal agenesis by E9.0, as demonstrated by models such as $T^{-/-}$ and *KD1-T*. Since the *KD3-T* knockdown model mainly exhibits defects in notochord and derived structures, but the hairpin is expressed ubiquitously, this supports that there is a higher requirement for T in maintaining notochord character than that needed for maintenance of the tailbud and resultant axial elongation.

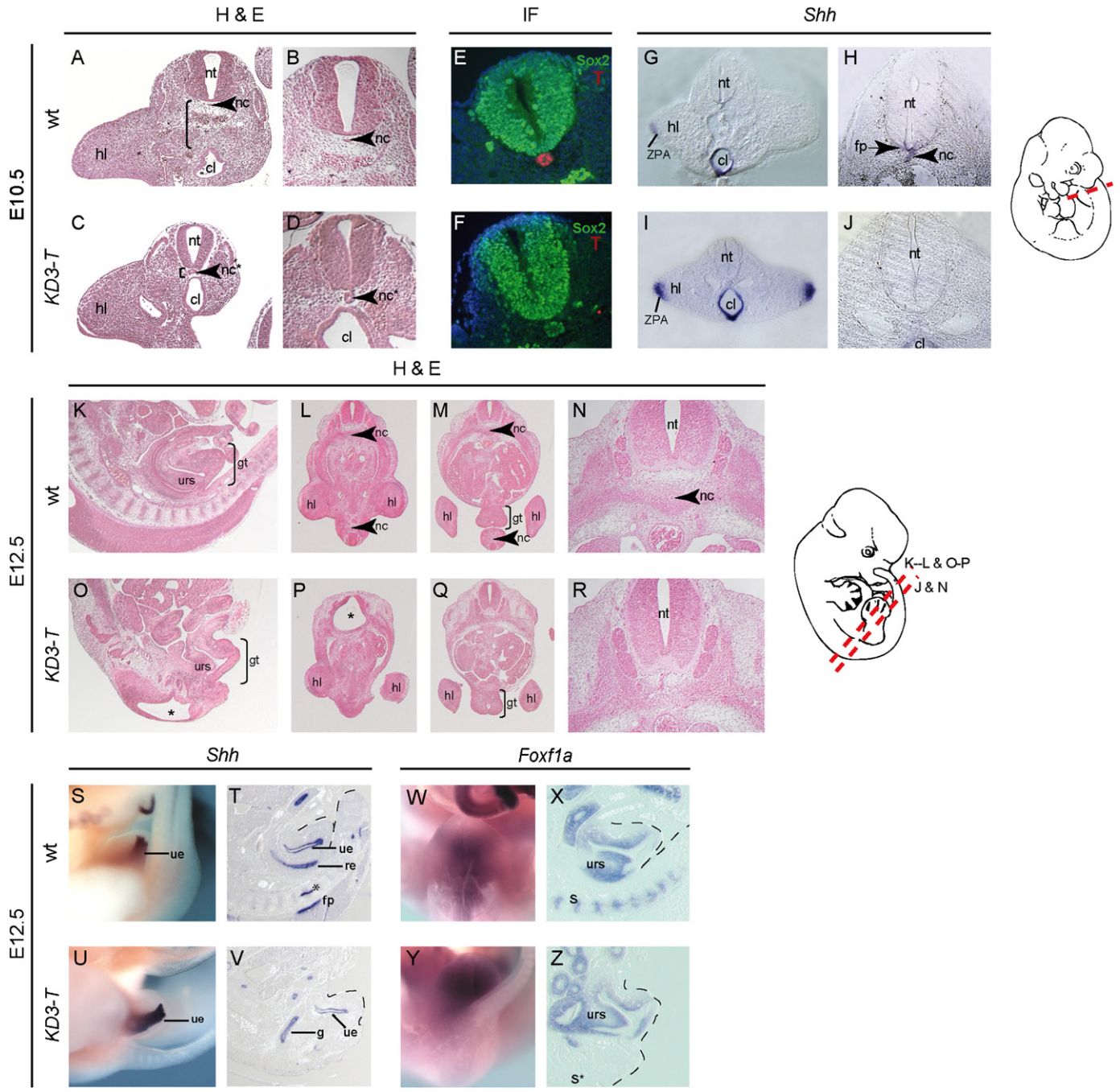

Fig. 2. Knockdown of *T* results in a failure to maintain the notochord. ((A)–(D)) Hematoxylin and eosin (H&E) staining of transverse sections at the hindlimb (hl) level in E10.5 wt ((A) and (B)) and *KD3-T* embryos ((C) and (D)) reveal that the notochord (nc) has an abnormal morphology (nc*) at this level in *KD3-T* embryos (arrowheads). Note also the lack of trunk mesenchyme ventral to the neural tube (nt) in the transgenic embryo (compare brackets in (A) and (C)). ((E) and (F)) Immunofluorescence (IF) at the level of the cloaca just caudal to the hindlimb for *T* (red) and the neural marker Sox2 (green) illustrates that the notochord no longer expresses *T*, and instead takes on a neural character. Nuclei were counterstained with DAPI (blue). ((G)–(J)) Vibratome sections following WISH for *Shh* show that the undifferentiated notochord structure and the floorplate (fp) in *KD3-T* embryos lacks *Shh*, although other domains of *Shh* expression, including the cloacal endoderm (cl) and Zone of Polarizing Activity (ZPA) in the limb bud are present. ((K)–(R)) Histology on midsagittal ((K) and (O)) and transverse ((L)–(N), (P)–(R)) sections at E12.5 show that the caudal region of *KD3-T* embryos is severely disrupted at this stage, but the genital tubercle (gt) appears normal. *KD3-T* embryos at this stage invariably display spina bifida (asterisk), loss of somites, and the dorsocaudal embryo is unstructured. At the level of the hindlimb the notochord has fully degenerated in the transgenic animals (arrowheads). Embryo illustrations to the right indicate the level of the sections. ((S)–(Z)) An examination of *Shh* ((S)–(V)) and *Foxf1a* expression ((W)–(Z)) by *in situ* hybridization on whole embryos and midsagittal sections at E12.5 reveals a normal distribution of transcripts for both genes in the endoderm and mesoderm of the genital tubercle, respectively. Expression of *Shh* is absent in the notochord (asterisk in T) and floorplate (fp) (compare (T) with (V)). *Foxf1a* expression is accordingly lost from the sclerotome ((X) and (Z), s/s*). Dotted lines mark the genital tubercle and anorectal groove. Note that the tail has been removed in (W) to allow for a view of the genital tubercle. g, gut; re, rectal epithelium; ue, urethral epithelium; urs, urorectal septum. (For interpretation of the references to color in this figure legend, the reader is referred to the web version of this article.)

KD3-T embryos exhibit increased cell death in caudal mesenchyme

The caudal phenotype of *KD3-T* embryos, including loss of somites and unstructured mesodermal tissue posterior to the hindlimb bud, is pronounced by E12.5. Although the phenotype is already discernible beginning at E10.5, induced *KD3-T* embryos have a normal number of somites when compared to their age-matched littermates at E9.5 and E10.5 (Vidigal et al., 2010 and

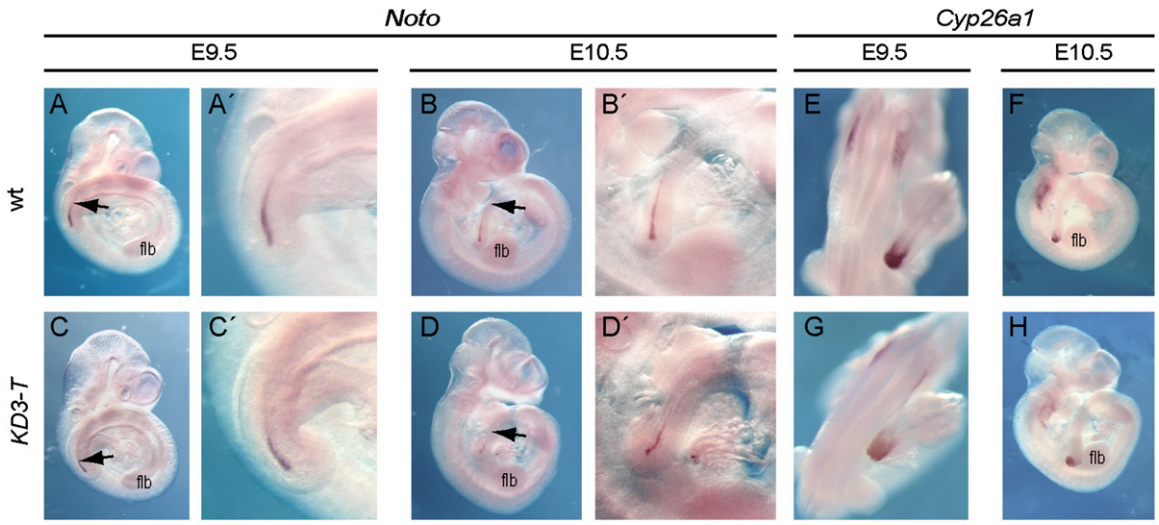

Fig. 3. In *KD3-T* embryos nascent notochord cells are present and expression of the tailbud marker *Cyp26a1* is maintained. ((A)–(H)) WISH expression of *Noto* ((A)–(D)) and *Cyp26a1* ((E)–(H)) at E9.5 and E10.5 in wt and *KD3-T* littermates. In ((A)–(D)) arrows point to the rostral limit of *Noto* expression, and enlargements of the tailbud are shown to the right. Embryos were cleared in 50% formamide/50% PBS after staining for better visualization of the notochord. flb, forelimb bud.

data not shown). This suggests that a loss of mesodermal tissue occurs between E10.5 (the first appearance of the phenotype) and E12.5 (when caudal somites are absent and the tail filament is present). In order to examine whether the loss of mesoderm observed at E12.5 was caused by increased cell death, we examined LysoTracker Red-stained *KD3-T* embryos and control littermates at E10.5 and E11.5 (Fig. 4). This analysis revealed a clear degeneration of somites and mesodermal tissue in *KD3-T* embryos at and below the lumbar level (Fig. 4C and F), further illustrating that notochordal T activity in the trunk and tail is essential for maintenance and survival of mesoderm cells.

The premise that an intact notochord is required to maintain somites is consistent with the phenotypes seen in various alleles of *T*, along with both the vestigial tail (*vt*) and Danforth's short tail (*Sd*) mice, as well as in embryos displaying an absence of *Shh* in the notochord. In the *vt* mutant model, which have been shown to be hypomorphic for *Wnt3a*, embryos display somite and caudal neural tube abnormalities as a result of loss of the notochord and improper specification of mesoderm (Greco et al., 1996; Yoshikawa et al., 1997). Somite number is found to be affected after E11.5 in *vt* embryos (Greco et al., 1996), and in *Sd* mutants the notochord degenerates by E9.5, but somites continue to form. They are eventually lost via apoptosis of epaxial myotome (Asakura and Tapscott, 1998). As previously mentioned, embryos lacking Shh signaling in the notochord show a similar phenotype to *KD3-T* with increased posterior cell death and presence of a tail filament (Choi and Harfe, 2011; Seifert et al., 2009).

Fate mapping and extirpation studies have indicated that the first somites formed are derived from the posterior node/anterior primitive streak region. As development proceeds and the primitive streak recedes and merges into the tailbud, the tailbud contributes all mesodermal precursors that generate the remaining somites (by the 24–26 somite stage or approximately E9.0) (Tam and Beddington, 1987, 1992; Tam et al., 2000; Tam and Tan, 1992). Accordingly, the loss of axial and paraxial mesoderm that we observe here is not likely to be the result of a general reduction in the generation or specification of mesoderm, since T is still present at sufficient levels in the tailbud for axial specification, but rather insufficient levels of T in the notochord which result in increased cell death. This argument is strengthened by both the observation that somites degenerate following surgical removal of the notochord in chicks (van Straaten and Hekking, 1991) and by the phenotype seen following loss of Hh signaling in the notochord, where embryos display increased cell death in the caudal region along with a tail filament (Choi and Harfe, 2011; Seifert et al., 2009) similar to what is seen in the *KD3-T* model. Since SHH is not involved in axial elongation or mesoderm specification, the defects seen following notochordal disruption of *Shh* result exclusively from impaired notochord development and signaling.

Axial skeletal defects observed in KD3-T embryos are consistent with loss of the differentiated notochord and resemble those of the caudal regression syndrome

The normal vertebral pattern in the mouse consists of seven cervical vertebrae (C1–C7), 13 thoracic vertebrae (T1–T13), seven of which are fused to the sternum, six lumbar (L1–L6), four sacral (S1–S4), and around 30 caudal vertebrae. Skeletons from nine *KD3-T* embryos (from three separate mating pairs) were compared with their wild-type littermates at E18.5. Although the gross morphology of the transgenic embryos was very similar, presenting with a tail filament and spina bifida occulta, the resulting skeletal phenotypes varied dramatically (Fig. 5A, Tg1 to Tg9). The vertebral column was generally arrested around the lumbar/sacral level with several poorly developed lumbar vertebrae and a sacral rudiment (6/9) (*e.g.*, Tg7, Fig. 5E–G). In one severe case the vertebral column ended after the third thoracic vertebra, although the ventral portion of 8 ribs were present (Tg1, Fig. 5H–J). The majority of the *KD3-T* embryos had no caudal vertebrae (7/9), and the remaining had only a few, malformed caudal vertebrae with an absence of sacral vertebrae (2/9). The anterior skeleton including the occipital bones of the skull (9/9) and the cervical vertebrae were normal, with the exception of a 30% incidence of C7→T1 homeotic transformations (3/9; 2 unilaterally and 1 bilaterally). The variation in axial defects observed here is similar to that seen in caudal regression syndrome patients, where the lumbar and sacral vertebrae are most often affected, with occasional involvement of thoracic segments (Boulas, 2009; Renshaw, 1978).

Since axial development in *T* mutants has been found to correlate with gene dosage (Yanagisawa, 1990), it is possible that the variable skeletal phenotypes observed here are the result of subtle timing of loss of T in the notochord after E8.5, which may fluctuate due to the nature of the shRNA-induced knockdown. Some variation in axial development has also been noted in

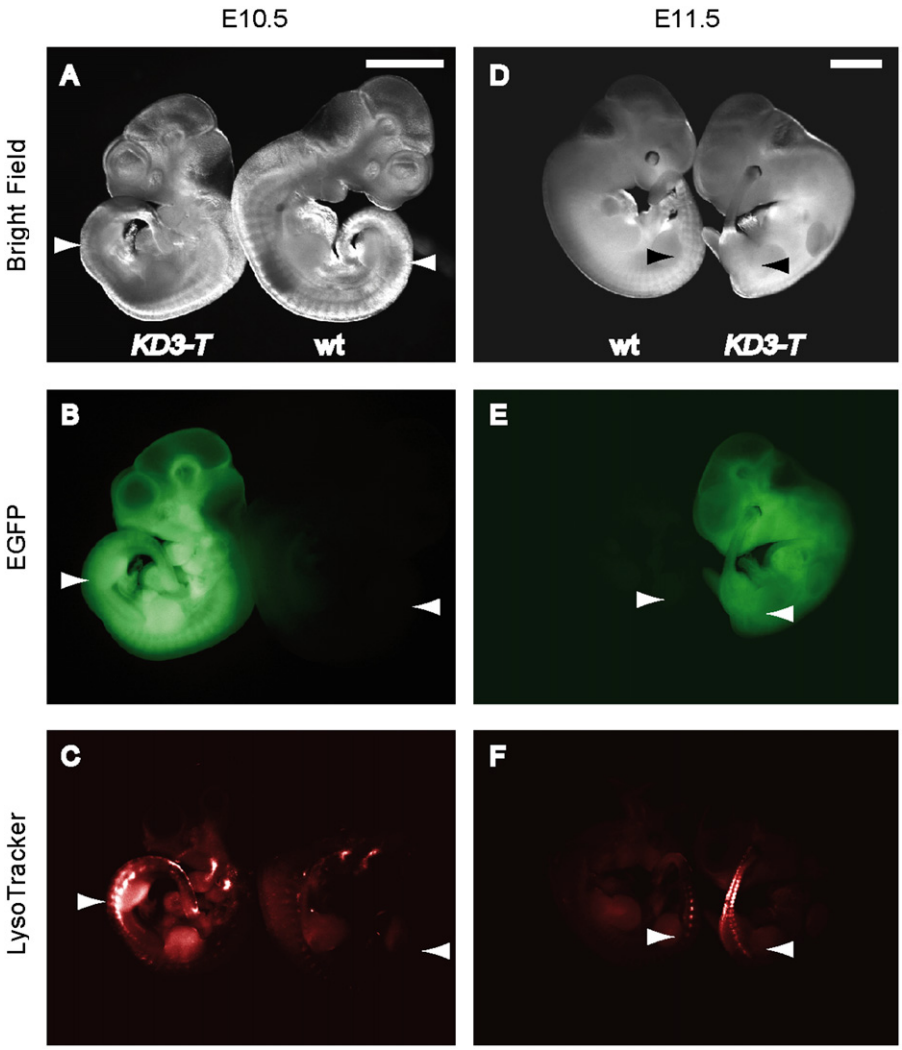

Fig. 4. Knockdown of T causes increased cell death posterior to the hindlimb. Cell death was assessed in wt and *KD3-T* transgenic littermates at E10.5 ((A)–(C)) and E11.5 ((D)–(F)). An increase in cell death via detection of LysoTracker Red was observed in *KD3-T* embryos posterior to the hindlimb level (marked by arrowheads) at both stages ((C) and (F)). Transgenic embryos were distinguishable by ubiquitous expression of EGFP ((B) and (E)) and bright field images are shown for reference ((A) and (D)). Scale bars represent 1 mm. (For interpretation of the references to color in this figure legend, the reader is referred to the web version of this article.).

various *T* allelic mutants, which suggests that these observed defects could also be caused by a more general mechanism with regards to the available amount of functional T protein. Animals which are heterozygous for *T* or various alleles of *T* survive long enough to allow for an examination of the skeletal phenotype. Axial defects in $T^{+/-}$ are variable and strongly affected by genetic background, but mainly confined to a shortened or absent tail, with very rare cases including defects in sacral vertebrae (Gruneberg, 1958). The *T* antimorphs T^{Wis} and T^{C} show a more severe phenotype. $T^{Wis}/+$ embryos have arrested notochord development at the lumbar/sacral level and a general loss of the vertebral structures below the sacrum (Kispert and Herrmann, 1994), and $T^{C}/+$ mutants present with vertebral malformations which can involve the thoracic region (Searle, 1966).

Vertebrae located at the thoracic level and more rostrally are derived from the primitive streak, whereas lumbar, sacral, and caudal vertebrae are derived from the tailbud (Greco et al., 1996). All somites initially develop in *KD3-T* embryos, as visualized by expression of *Uncx* (Vidigal et al., 2010). Therefore, the range of axial defects observed in *KD3-T* embryos at later stages likely result from an inability to maintain the notochord resulting in varying amounts of degeneration of the paraxial mesenchyme.

Gross morphological examination of KD3-T embryos at later stages reveals secondary urorectal anomalies

Several mouse models have been examined which exhibit caudal and/or notochord defects, and these are often accompanied by secondary urorectal anomalies (for examples see Gluecksohn-Schoenheimer, 1943; Nakata et al., 2009; Padmanabhan, 1998; Seifert et al., 2009; van de Ven et al., 2011). Moreover, the axial defects we observed strongly resembled those present in caudal regression syndrome, where posterior skeletal abnormalities are associated with urorectal malformations (Boulas, 2009; Duhamel, 1961; Renshaw, 1978). This prompted us to examine *KD3-T* embryos with a focus on the incidence of urogenital and anorectal malformations. At later stages of development (E13.5-P0), surviving knockdown embryos consistently displayed defects in caudal morphology, including caudal regression with a tail filament (Fig. 6A–C). We additionally observed various anorectal defects including imperforate anus (Fig. 6B), and anal stenosis (Fig. 6C) and, although the morphology of the external genitalia was for the most part normal, hypospadias was noted in one case (Fig. 6B).

Urorectal malformations in mice exhibiting caudal regression phenotypes mainly arise via a general loss of caudal tissue, since

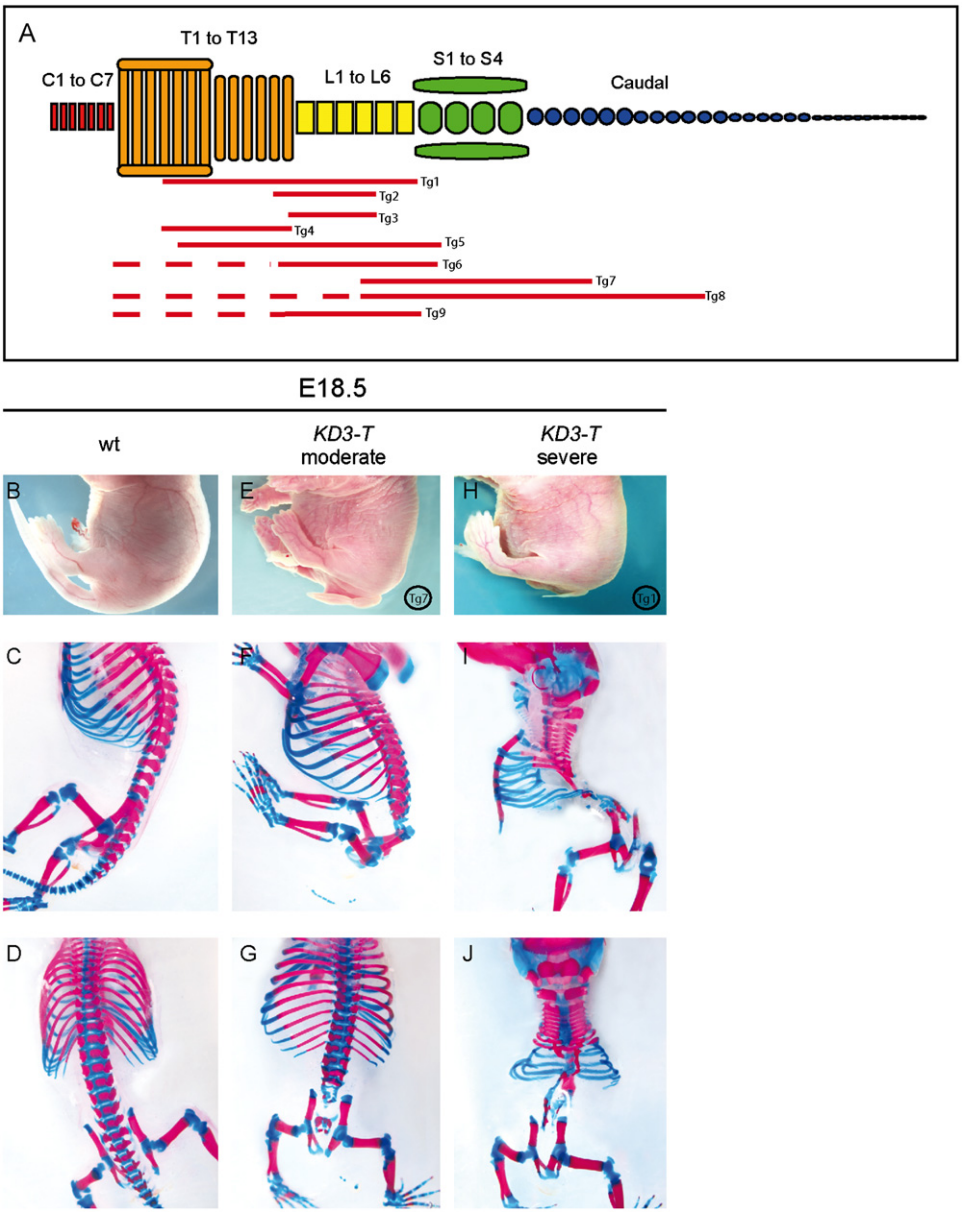

Fig. 5. *KD3-T* embryos present with axial skeletal defects of varying severity. (A) Diagram illustrating the variance in axial skeletal defects observed in nine *KD3-T* fetuses at E18.5. The normal skeletal pattern is shown at the top with 7 cervical, 13 thoracic, 6 lumbar, 4 sacral, and ~30 caudal vertebrae. Tg1 to Tg9 correspond to the individual skeletons examined with solid red lines marking abnormal formation or absence of vertebrae, and dashed lines indicating animals which demonstrated cervicothoracic posterior homeotic transformations. ((B)–(J)) Gross and skeletal morphology of a wt fetus ((B)–(D)), compared to a *KD3-T* fetus with a moderate phenotype ((E)–(G); Tg7), and an example with a severe phenotype ((H)–(J); Tg1). The gross morphologies of the Tg7 (moderate) and Tg1 (severe) fetuses were nearly indistinguishable (compare E with H), but development of the vertebral column stops at L4 in the moderate case, with several small caudal vertebra also formed ((F) and (G)), whereas the severe case shows a loss of vertebrae posterior to the third thoracic segment, with only a thin bony remnant extending to the sacral level ((I) and (J)). Forelimbs were removed from some embryos for imaging, but it should be noted that appendicular structures appeared normal in all cases. (For interpretation of the references to color in this figure legend, the reader is referred to the web version of this article.)

development of the urorectal system involves tissues originating from all 3 germ layers: the lateral plate mesoderm-derived urorectal septum, the endodermal urethral and rectal epithelial surface, and surface ectoderm of the cloacal membrane. However, malformations of the urorectal region such as imperforate anus and hypospadias can also derive exclusively from improper development/progression of the mesodermally-derived urorectal septum (urs), which divides the cloaca into the urethra and rectum around E12.5–E13.5 (Perriton et al., 2002). The importance of T in mesoderm formation has been well noted, and the reduction in paraxial mesoderm at early stages (*i.e.*, E10.5, Fig. 2C and D) suggested to us that there might be an effect of loss of mesoderm on the formation and progression of mesoderm-derived urs. This improper progression of the urs was confirmed by examining sagittal sections through the urorectal region between E12.5 and E18.5 (Fig. 6 and data not shown). Patterning and outgrowth of the genital tubercle itself, however, was found to be normal, as verified by examining the expression of markers for various components of the genital tubercle, including *Hoxd13* (distal genital tubercle mesenchyme, Fig. 7A), *Sall3* (ventral pericloacal mesenchyme and urethral plate, Fig. 7B), along with *Dlx5* and *Bmp7* (distal genital tubercle mesenchyme, data not shown).

Conclusions and perspectives

It is quite possible that the original function of the *T* gene was to establish the notochord, and its function in maintaining

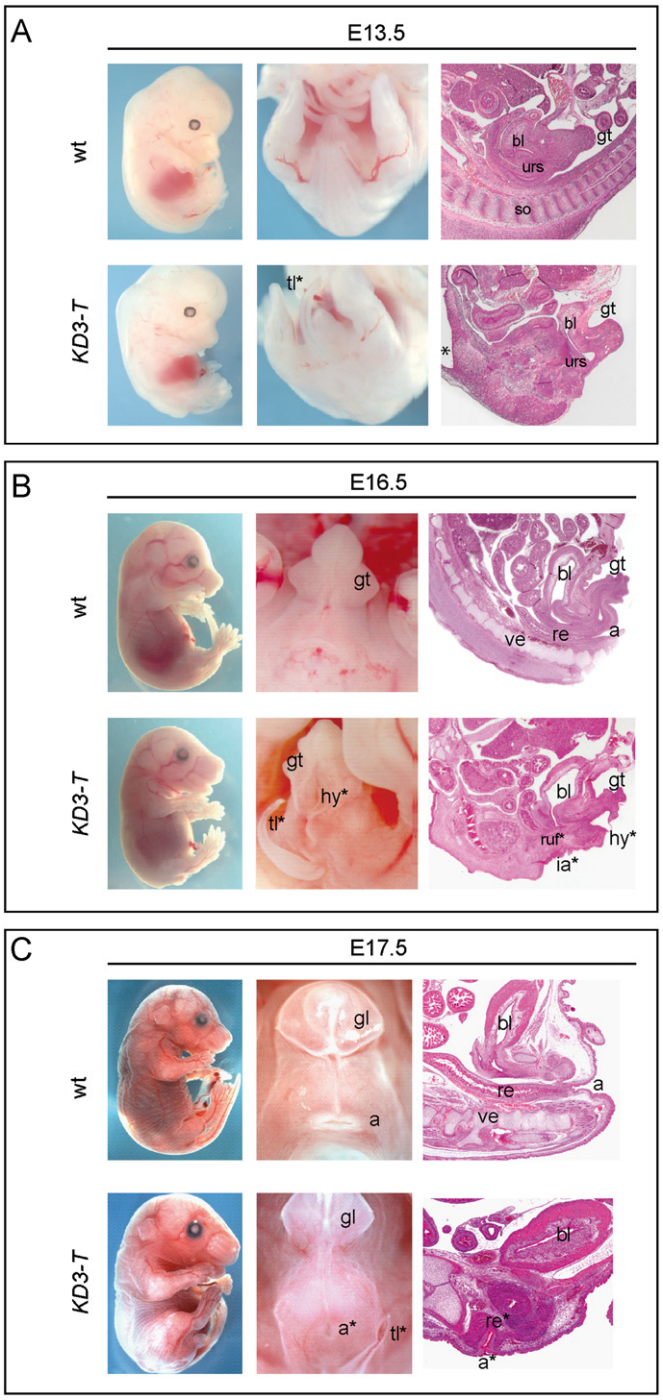

Fig. 6. Secondary urorectal anomalies manifest from insufficient T. ((A)–(C)) Gross morphological and histological analyses of *KD3-T* and wt littermates at E13.5 (A), E16.5 (B), and E17.5 (C). Embryos consistently displayed caudal malformations, spina bifida (asterisk), and presence of a tail rudiment (tl*). Absence of somites (so) and corresponding loss of vertebrae (ve) results in tissue disorganization in the caudal region of *KD3-T* embryos. Secondary anorectal defects were often observed at later stages of development, and included rectal and anal atresia (re* and a*), and recto-urethral fistula (ruf*) with imperforate anus (ia*). Morphology of the genital tubercle (gt) was mostly unaffected, although hypospadias (hy*) was observed in one instance (B). a, anus; bl, bladder; gl, glans; re, rectum; urs, urorectal septum.

posterior mesoderm was secondarily acquired for posterior extension of the body axis. It has been understandably difficult to separate the role for T in these two structures since the morphogenesis of the notochord and posterior axis are closely coupled in time and space. This is especially true at early developmental stages when the streak is continuous with the notochordal plate. Thus, although our model provides interesting insight into the role of functional T in notochord maintenance, we will only be able to fully differentiate the role for T in the notochord from that in axis extension by affecting T function in these separate tissues, or at various axial levels and developmental times. The overarching result of T knockdown in the *KD3-T* model, however, is increased cell death in the trunk and tail, leading to the appearance of an unstructured caudal trunk, and subsequent skeletal and urorectal defects (Fig. 8).

It has been noted that *T*-null mutants have an abnormal notochord in rostral regions at E8.0 (Yamaguchi et al., 1999), and inbred $T^{+/-}$ embryos can have an abnormal notochord which is absent in the caudal-most region (Chesley, 1935; Cogliatti, 1986; Gruneberg, 1958). Analysis of the *KD3-T* model illustrates that sufficient levels of notochordal T are required for differentiation of a mature notochord structure which retains mesodermal character, as opposed to adopting a neural character. Several mutants have been described which display abnormal notochord structures with neural character—so-called 'ectopic neural structures'. *Wnt3a* mutants fail to express *T* and display diplomyelia, *i.e.*, presence of a second neural structure (Yamaguchi et al., 1999), but they also fail to form both a tailbud and somites caudal to approximately somite 9 (Yoshikawa et al., 1997). This is a stronger phenotype than the one we observe here; likely because *T* is also absent from the tailbud in *Wnt3a*-null embryos. *Tbx6* is expressed in the presomitic mesoderm surrounding the notochord, and maintenance of its expression has been found to be dependent on *T* (Chapman et al., 1996). *Tbx6* mutants lack paraxial mesoderm posterior to the forelimbs and have three correctly patterned neural tubes (Chapman and Papaioannou, 1998). In addition, it has been long noted that various T mutants have defects in and loss of somites. Since T protein is undetected in the somites themselves, expression of T in the notochord must regulate somite specification via regulation of another signaling molecule from the notochord (Herrmann, 1991). It is very likely that this signal is Shh, which initiates sclerotome development (Fan et al., 1995; Fan and Tessier-Lavigne, 1994; Johnson et al., 1994), however, the downstream mechanisms involved in notochord signaling in mice, especially via *T*, are still not entirely clear. Even though much is known about the requirement for T-box genes during development, surprisingly little is known about their *bona fide* downstream targets (Showell et al., 2004). In the *KD3-T* model the caudal notochord is initiated but fails to express *T* or *Shh* (Figs. 1–3), resulting in a phenotype resembling that seen after ablation of *Shh* at E10.5 (Seifert et al., 2009). Removal of *Shh* either generally (Chiang et al., 1996), or specifically from the notochord (Choi and Harfe, 2011), has been shown to not disrupt formation of the notochord structure, unlike what is seen here. Also, *Shh* is required in formation of epaxial myotome (Chiang et al., 1996), but dermomyotome becomes dermis and musculature, whereas sclerotome becomes ribs and vertebrae—and *KD3-T* embryos are missing the latter but not the former. Taken together, this suggests that T is responsible for perdurance of the notochord upstream of Shh.

Caudal regression phenotypes accompanied by anorectal and urogenital malformations in the mouse form the basis for the "uro-rectal-caudal syndrome" (Gruneberg, 1952). This uro-rectal-caudal phenotype was first described as a recessive mutation (*u*) spontaneously arising from the Line A tailless mice, and was complemented by intercrosses with *T* mice (Dunn and Gluecksohn-Schoenheimer, 1947). The mutation resulted in tailless offspring that also presented in rare cases with imperforate anus. This was accompanied by defects of the genitals, gut, and kidneys. Urorectal malformations are among the most common human birth defects, with prevalence estimates varying between 1 in 2500 live births (for mild forms) to 1 in 200,000 (for more severe forms) (Feldkamp et al., 2011; Siffel et al., 2011; Stoll et al., 2007). The incidence of babies born with

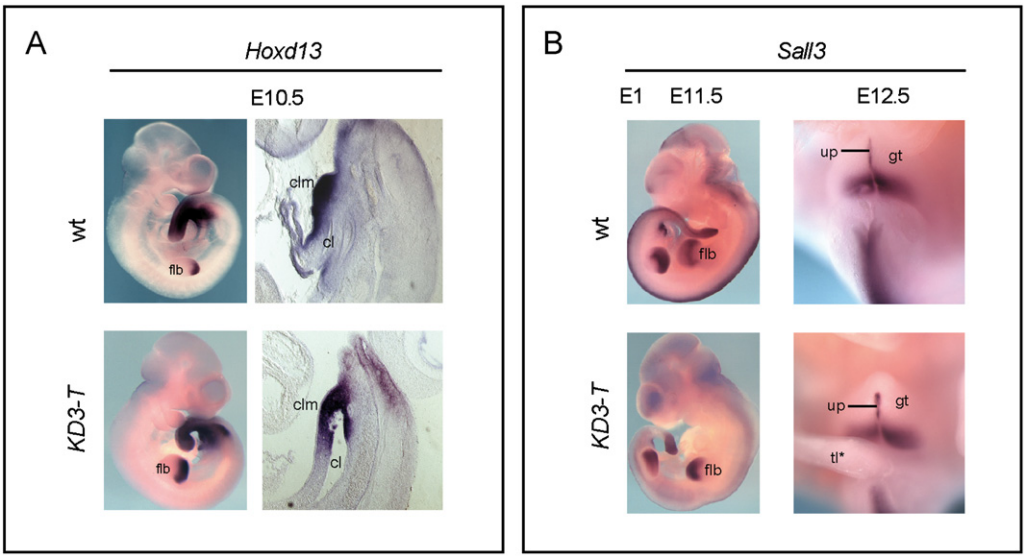

Fig. 7. Patterning of the genital tubercle is unaffected in *KD3-T* embryos. (A) WISH and subsequent vibratome sectioning of *KD3-T* and wt littermates at E10.5 revealed that distribution of *Hoxd13*, a marker of the cloacal membrane (clm) and distal genital mesenchyme, was unaffected in the transgenic embryos. (B) *Sall3* expression in *KD3-T* embryos was comparable to wt in the ventral genital tubercle (gt) and urethral plate (up) at E11.5 and E12.5, but was not expressed in the neural tube of the rudimentary tail filament (tl*) in transgenic embryos (note that the tail has been removed in the wild type case). cl, cloaca; flb, forelimb bud.

caudal regression syndrome has been estimated to be around 1 in 60,000 births (Singh et al., 2005; Stevenson et al., 1986). Incidence is 200 times more likely in diabetic mothers for reasons that remain unclear, but since only 20% of all caudal regression patients are born to diabetic mothers, a more complex etiology persists (Boulas, 2009; Singh et al., 2005). Since our model provides a robust and reproducible phenotype for caudal regression accompanied by urorectal defects, it can be used to examine the link between loss of caudal mesenchyme and associated anorectal and genital anomalies. More importantly, since *KD3-T* transgenic embryos can be easily identified by EGFP expression before the phenotype is evident, this allows for analysis of early molecular events—something that has presented a challenge in the past for murine models of caudal regression where the nature of the mutation remains unknown (such as *u* and *Sd*), and when mutants are identifiable only at mid-gestational stages (such as for T^{Wis} and T^{C}).

The suggestion that BRACHYURY may be involved in sacral agenesis and caudal regression in human patients has been examined, with debatable findings. In one study, three unrelated patients within a sample of 50 subjects with documented congenital vertebral anomalies were found to harbor heterozygosity of a 1013C > T variant of the *T* gene (Ghebranious et al., 2008). However, the variant was found to be passed on in each case from a clinically unaffected parent. Additionally, an earlier study of 28 patients with sacral agenesis revealed that the gene is highly polymorphic. Although amino acid substitutions were found in the *BRACHYURY* coding sequence, it was ruled out as a major contributing factor (Papapetrou et al., 1999). The caveat is that in both of these studies only the coding sequence and/or immediate 500 bp upstream of the start site were examined. This represents the so-called 'T-streak' promoter which directs expression only in the primitive streak and derivatives (Clements et al., 1996). Studies of the *T* promoter have revealed that the notochord-specific region is either *trans* or long-range *cis*-acting (Clements et al., 1996; Wu et al., 2007), which would complicate the ability to locate a causative mutation if it affected the notochord expression of *T* specifically. Our results imply that a mutation in the notochord-specific promoter/enhancer element of *T* could contribute to sacral agenesis along with urorectal anomalies.

Experimental procedures

Animals

Generation of the transgenic embryos containing an shRNAmir directed against *Brachyury* have been previously described (Vidigal et al., 2010). The transgene was subsequently introduced into ES cells of a 129S6/SvEvTac × C57BL/6NCr F1 background and used to generate chimeras. Germline transmission was validated and the line was propagated on a C57BL/6 J background (*Gt(ROSA)26Sor*$^{tm3(tetO-EGFP,-RNAi:T)Bgh}$ (MGI:5297100)). Genotyping was performed by Southern analysis as described (Vidigal et al., 2010). All experiments described in this work use *KD3-T* embryos derived from C57BL/6 J transgenic males mated to NMRI wild-type females. The transgene was induced by Dox treatment (4 mg/ml, Sigma) provided in a 1% sucrose solution to pregnant dams in the drinking water. Timed matings were calculated designating noon of the day a vaginal plug was detected as E0.5. Dox was provided *ad libitum* from detection of the plug, and continuously until embryos were harvested. Thus, knockdown of *T* will occur continuously until analysis (see Vidigal et al., 2010 for further details). Embryos harboring the transgene were ascertained by monitoring EGFP at E9.5 and E10.5, and phenotypically from E11.5 onward. *T* heterozygote embryos were obtained from matings of $T^{+/-}$ NMRI males (identified by short tail) crossed to wild-type C57BL/6 females. Embryos were genotyped from yolksac DNA by genomic qPCR using primers within the T-streak promoter (F: 5′CCCGGCCAGTCTGATATG; R: 5′CCCATAAATACAGCCGAGGTGG), and levels were normalized to *Msgn* (F: 5′GGAACTTTGCACAGGAGGAG; R: 5′TGGGTAACGGCTTCCTAATG). All animal experiments were performed in ethical accordance with protocols approved by the Berlin Animal Care Authorities (LAGeSo).

qPCR and immunoblotting

Embryos were generated as above and collected at E9.5 and E10.5 into PBS. Wildtype and *KD3-T* littermates were separated using detection of EGFP, and $T^{+/-}$ embryos were genotyped using qPCR to determine presence of the *T* promoter. Tailbud and notochord samples (anterior to the tailbud) were dissected using a flamed tungsten needle. For qPCR analysis biological triplicates

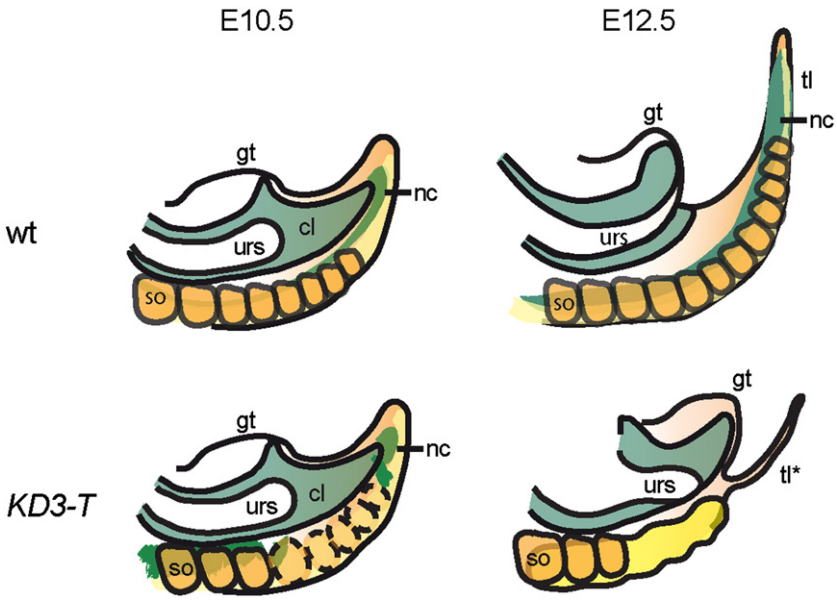

Fig. 8. *KD3-T* embryos fail to maintain the notochord and exhibit a phenotype resembling caudal regression syndrome. The diagram illustrates the morphological events leading to caudal and secondary urorectal malformations in *KD3-T* embryos. By E10.5 the notochord fails to differentiate, resulting in increased cell death at and below the level of the hindlimbs. By E12.5 the sclerotome is absent and the structural integrity of the caudal embryo has been disrupted, resulting in spina bifida and aberrant tissue morphology at the sacral level (yellow), along with an arrest of tail development. The lack of somites and subsequent vertebrae in the caudal embryo results in improper progression of the urs and resultant urorectal malformations. This combination of variable loss of vertebrae and accompanying urorectal malformations resembles phenotypes associated with caudal regression syndrome in humans. cl, cloaca; nc, notochord; gt, genital tubercle; so, somites; tl, tail, tl*, tail filament; urs, urorectal septum. (For interpretation of the references to color in this figure legend, the reader is referred to the web version of this article.)

of tissue from 3 embryos for each wt and *KD3-T* littermates or biological replicates of 3 $T^{+/-}$ tissues were pooled, and total RNA was extracted using the Qiagen RNeasy Micro Kit according to manufacturer's instructions. Superscript II (Invitrogen) was then used to generate cDNA using random hexamer priming. Real-time RT-PCR was performed for *T* (F: 5′CAGCTGTCTGGGAGCCTGG; R: 5′TGCTGCCTGTGAGTCATAAC) and levels normalized to expression of *Pmm2* (F: 5′AGGGAAAGGCCTCACGTTCT; R: 5′AATACCGCTTATCCCATCCTTCA) on a StepOnePlus™ Real-Time PCR System (Life Technologies) using GoTaq® qPCR Master Mix (Promega). For immunoblot analysis twenty-four samples from each tissue and age for wt and *KD3-T*, or 12 samples for $T^{+/-}$, were collected from separate matings (6 embryos per mating), and pooled into RIPA Buffer (50 mM Tris (pH8.0), 150 mM NaCl, 1% NP40, 0.25% Na-DOC, 0.1% SDS, 1 mM EDTA) plus Complete Protease Inhibitor Cocktail (Roche) for lysis. Lysates were collected into fresh tubes and total protein was measured by spotting onto nitrocellulose and staining with amido black. Two micrograms of protein for each sample was separated by SDS-PAGE, and blotted onto nitrocellulose membrane. The membrane was blocked using TBST containing 5% milk powder (Sigma), and incubated with primary antibodies overnight at 4 °C in blocking solution (rabbit anti-mouse T (1:4000) (Kispert and Herrmann, 1994) or rabbit anti-mouse histone H3 (Abcam ab1791, 1:10000)). Following several washes in TBST, secondary antibody incubation was carried out for 1 h at room temperature (ECL™ donkey anti-rabbit HRP-conjugated IgG, GE Healthcare (1:10000)). Chemiluminescence detection was carried out using the Lumigen™ TMA-6 kit (GE Healthcare) according to manufacturer's instructions, and signals captured onto Amersham Hyperfilm ECL film (GE Healthcare). Densitometry was performed using Image J analysis software (NIH).

Skeletal processing

Fetuses were collected at E18.5, skinned and eviscerated in PBS, and fixed overnight in 100% ethanol. Cartilage and bone were stained with 0.015% alcian blue (Sigma) and 0.015% alizarin red (Sigma) in 1% KOH, respectively, following standard procedures (Jegalian and De Robertis, 1992). Skeletons were subsequently cleared using several changes of 50% glycerol/1% KOH and stored in 80% glycerol until imaged.

Whole-mount in situ hybridization

Whole-mount *in situ* hybridization (WISH) was performed according to standard protocol (Chotteau-Lelievre et al., 2006). Antisense riboprobes were synthesized using the appropriate RNA polymerase and a nucleotide mix containing digoxigenin-11-UTP (Roche Diagnostics). Following probe hybridization and washes, an Anti-DIG antibody conjugated to alkaline phosphatase (AP) (Roche) was incubated with embryos overnight at 4 °C, and detection of AP activity was carried out using BCIP/NBT (Sigma) or BM Purple (Roche). For each probe, embryos were processed concurrently and staining reaction times were maintained between transgenic and control embryos, in order to limit variation in signal intensity. At least 3 control and transgenic embryos were examined for each gene and stage, and figures depict representative staining. Following staining, some specimens were post-fixed overnight in 4% PFA and vibratome sectioned (35 μm thickness). Probe templates were obtained from our in-house MAMEP collection (http://mamep.molgen.mpg.de) with the exception of the template for *Noto*, which was a kind gift from Achim Gossler and has been previously described (Abdelkhalek et al., 2004).

Histology

Embryos were fixed overnight in 4% PFA and processed into paraffin wax. Sections were cut at a thickness of 5 μm. Hematoxylin and eosin staining was performed according to standard procedures. *In situ* hybridization was performed on paraffin sections (5 μm) according to the protocol from Chotteau-Lelievre et al. (2006) with minor modifications, and detection of AP activity was visualized using BM Purple (Roche Diagnostics).

Following staining, slides were quickly dehydrated in 80% and then 100% ethanol, cleared twice for 1 min in xylene (Roth) and coverslips were mounted with Entellan mounting medium (Merck). Images were captured using AxioVision software (Zeiss) with a Zeiss AxioCam and SteREO Discovery.V12 microscope. At least 3 embryos were analyzed at each stage shown for transgenic and wild type and representative images are provided.

Immunofluorescence

Paraffin sections of 5 μm thickness were de-paraffinized using xylene, and then rehydrated using an ethanol series. Antigen retrieval was performed by boiling in 0.01 M citrate buffer (pH6.0) for 10 min. Sections were blocked for 1 h at room temperature in 1% BSA/10% lamb serum and then incubated overnight at 4 °C with primary antibodies. Antibodies used were mouse monoclonal anti-SOX2 (Abcam ab79351) (1:300) and rabbit anti-mouse T (Kispert and Herrmann, 1994) (1:500). Secondary antibody incubation using goat anti-mouse Alexa Fluor-488 conjugated and goat anti-rabbit Alexa Fluor-594-conjugated IgG (both at 1:1000; Invitrogen Molecular Probes) was performed for 60 min at room temperature in the dark. Slides were mounted with Vectashield® Mounting Medium containing DAPI (Vector) and images were captured on a Zeiss Observer.Z1 microscope and analyzed using the AxioVision 4.6 software. Sections at the level surrounding the hindlimb bud at E10.5 were examined for at least 4 of each wildtype and *KD3-T* embryos. Exposure times were normalized and representative images are shown.

Analysis of apoptosis in whole embryos

Embryos were collected into warm PBS and stained with 5 μM LysoTracker Red (Invitrogen) in PBS at 37 °C for 45 min. Following staining, embryos were washed once with PBS and fixed in 4% PFA overnight. They were then rinsed three times with PBS, and imaged immediately. At least 15 embryos of each age were examined for both control and transgenic littermates. Images were captured using a Leica MZ16FA fluorescence stereo microscope and processed using Leica Application Suite. Representative images are shown using littermate references.

Acknowledgments

T.P., A.K., B.G.H., and L.W. are members of the German Network for the Systematic Investigation of the Molecular Causes, Clinical Implications and Psychosocial Outcome of Congenital Uro-Rectal Malformations (CURE-Net) Consortium. We would like to thank Eileen Jungnickel and Sonja Banko for expert animal husbandry, and Stefanie Wolter for technical assistance. Thanks also to Lisette Lange for assistance with imaging, and to Matthias Marks, Arica Beisaw, and Don Cameron for comments on the manuscript and useful discussions regarding this work. This research was funded by the German Federal Ministry of Education and Research (BMBF) Federal Funding Program for Rare Diseases; Grant number 01GM08107.

References

Abdelkhalek, H.B., Beckers, A., Schuster-Gossler, K., Pavlova, M.N., Burkhardt, H., Lickert, H., Rossant, J., Reinhardt, R., Schalkwyk, L.C., Muller, I., Herrmann, B.G., Ceolin, M., Rivera-Pomar, R., Gossler, A., 2004. The mouse homeobox gene not is required for caudal notochord development and affected by the truncate mutation. Gene. Dev. 18, 1725–1736.

Abu-Abed, S., Dolle, P., Metzger, D., Beckett, B., Chambon, P., Petkovich, M., 2001. The retinoic acid-metabolizing enzyme, CYP26A1, is essential for normal hindbrain patterning, vertebral identity, and development of posterior structures. Gene. Dev. 15, 226–240.

Ando, T., Semba, K., Suda, H., Sei, A., Mizuta, H., Araki, M., Abe, K., Imai, K., Nakagata, N., Araki, K., Yamamura, K., 2011. The floor plate is sufficient for development of the sclerotome and spine without the notochord. Mech. Dev. 128, 129–140.

Asakura, A., Tapscott, S.J., 1998. Apoptosis of epaxial myotome in Danforth's short-tail (Sd) mice in somites that form following notochord degeneration. Dev. Biol. 203, 276–289.

Boulas, M.M., 2009. Recognition of caudal regression syndrome. Adv. Neonatal Care 9, 61–69, quiz 70-61.

Chapman, D.L., Agulnik, I., Hancock, S., Silver, L.M., Papaioannou, V.E., 1996. Tbx6, a mouse T-Box gene implicated in paraxial mesoderm formation at gastrulation. Dev. Biol. 180, 534–542.

Chapman, D.L., Papaioannou, V.E., 1998. Three neural tubes in mouse embryos with mutations in the T-box gene Tbx6. Nature 391, 695–697.

Chesley, P., 1935. Development of the short-tailed mutant in the house mouse. J. Exp. Zool. 70, 429–435.

Chiang, C., Litingtung, Y., Lee, E., Young, K.E., Corden, J.L., Westphal, H., Beachy, P.A., 1996. Cyclopia and defective axial patterning in mice lacking Sonic hedgehog gene function. Nature 383, 407–413.

Choi, K.S., Harfe, B.D., 2011. Hedgehog signaling is required for formation of the notochord sheath and patterning of nuclei pulposi within the intervertebral discs. Proc. Nat. Acad. Sci. U.S.A. 108, 9484–9489.

Chotteau-Lelievre, A., Dolle, P., Gofflot, F., 2006. Expression analysis of murine genes using *in situ* hybridization with radioactive and nonradioactively labeled RNA probes. Methods Mol. Biol. 326, 61–87.

Clements, D., Taylor, H.C., Herrmann, B.G., Stott, D., 1996. Distinct regulatory control of the Brachyury gene in axial and non-axial mesoderm suggests separation of mesoderm lineages early in mouse gastrulation. Mech. Dev. 56, 139–149.

Cogliatti, S.B., 1986. Diplomyelia: caudal duplication of the neural tube in mice. Teratology 34, 343–352.

Dietrich, S., Schubert, F.R., Lumsden, A., 1997. Control of dorsoventral pattern in the chick paraxial mesoderm. Development 124, 3895–3908.

Dobrovolskaïa-Zavadskaïa, N., 1927. Sur la mortification spontanee de la queue chez la souris nouveau-nee et sur l'existence d'un caractere (facteur) hereditaire ''non-viable''. C. R. Seances Soc. Biol. Fil. 97, 114–116.

Duhamel, B., 1961. From the mermaid to anal imperforation: the syndrome of caudal regression. Arch. Dis. Child. 36, 152–155.

Dunn, L.C., Gluecksohn-Schoenheimer, S., 1947. A new complex of hereditary abnormalities in the house mouse. J. Exp. Zool. 104, 25–51.

Fan, C.M., Porter, J.A., Chiang, C., Chang, D.T., Beachy, P.A., Tessier-Lavigne, M., 1995. Long-range sclerotome induction by sonic hedgehog: direct role of the amino-terminal cleavage product and modulation by the cyclic AMP signaling pathway. Cell 81, 457–465.

Fan, C.M., Tessier-Lavigne, M., 1994. Patterning of mammalian somites by surface ectoderm and notochord: evidence for sclerotome induction by a hedgehog homolog. Cell 79, 1175–1186.

Feldkamp, M.L., Botto, L.D., Amar, E., Bakker, M.K., Bermejo-Sanchez, E., Bianca, S., Canfield, M.A., Castilla, E.E., Clementi, M., Csaky-Szunyogh, M., Leoncini, E., Li, Z., Lowry, R.B., Mastroiacovo, P., Merlob, P., Morgan, M., Mutchinick, O.M., Rissmann, A., Ritvanen, A., Siffel, C., Carey, J.C., 2011. Cloacal exstrophy: an epidemiologic study from the International Clearinghouse for Birth Defects Surveillance and Research. Am. J. Med. Genet. C Semin. Med. Genet. 157C, 333–343.

Fujimoto, H., Yanagisawa, K.O., 1983. Defects in the archenteron of mouse embryos homozygous for the T-mutation. Differentiation 25, 44–47.

Ghebranious, N., Blank, R.D., Raggio, C.L., Staubli, J., McPherson, E., Ivacic, L., Rasmussen, K., Jacobsen, F.S., Faciszewski, T., Burmester, J.K., Pauli, R.M., Boachie-Adjei, O., Glurich, I., Giampietro, P.F., 2008. A missense T (Brachyury) mutation contributes to vertebral malformations. J. Bone Miner. Res. 23, 1576–1583.

Gluecksohn-Schoenheimer, S., 1938. The development of two tailless mutants in the house mouse. Genetics 23, 573–584.

Gluecksohn-Schoenheimer, S., 1943. The morphological manifestations of a dominant mutation in mice affecting tail and urogenital system. Genetics 28, 341–348.

Gluecksohn-Schoenheimer, S., 1944. The development of normal and homozygous Brachy (T/T) mouse embryos in the extraembryonic coelom of the chick. Proc. Nat. Acad. Sci. U.S.A. 30, 134–140.

Greco, T.L., Takada, S., Newhouse, M.M., McMahon, J.A., McMahon, A.P., Camper, S.A., 1996. Analysis of the vestigial tail mutation demonstrates that Wnt-3a gene dosage regulates mouse axial development. Gene. Dev. 10, 313–324.

Gruneberg, H., 1952. The Genetics of the Mouse, (second ed.) Martinus Nijhof, The Hague.

Gruneberg, H., 1958. Genetical studies on the skeleton of the mouse. XXIII. The development of brachyury and anury. J. Embryol. Exp. Morphol. 6, 424–443.

Haraguchi, R., Motoyama, J., Sasaki, H., Satoh, Y., Miyagawa, S., Nakagata, N., Moon, A., Yamada, G., 2007. Molecular analysis of coordinated bladder and urogenital organ formation by hedgehog signaling. Development 134, 525–533.

Herrmann, B.G., 1991. Expression pattern of the Brachyury gene in whole-mount TWis/TWis mutant embryos. Development 113, 913–917.

Herrmann, B.G., Labeit, S., Poustka, A., King, T.R., Lehrach, H., 1990. Cloning of the T gene required in mesoderm formation in the mouse. Nature 343, 617–622.

Jegalian, B.G., De Robertis, E.M., 1992. Homeotic transformations in the mouse induced by overexpression of a human Hox3.3 transgene. Cell 71, 901–910.

Johnson, R.L., Laufer, E., Riddle, R.D., Tabin, C., 1994. Ectopic expression of Sonic hedgehog alters dorsal–ventral patterning of somites. Cell 79, 1165–1173.
Kispert, A., Hermann, B.G., 1993. The Brachyury gene encodes a novel DNA binding protein. Embo. J. 12, 4898–4899.
Kispert, A., Herrmann, B.G., 1994. Immunohistochemical analysis of the Brachyury protein in wild-type and mutant mouse embryos. Dev. Biol. 161, 179–193.
MacLean, G., Abu-Abed, S., Dolle, P., Tahayato, A., Chambon, P., Petkovich, M., 2001. Cloning of a novel retinoic-acid metabolizing cytochrome P450, Cyp26B1, and comparative expression analysis with Cyp26A1 during early murine development. Mech. Dev. 107, 195–201.
Monkley, S.J., Delaney, S.J., Pennisi, D.J., Christiansen, J.H., Wainwright, B.J., 1996. Targeted disruption of the Wnt2 gene results in placentation defects. Development 122, 3343–3353.
Nakata, M., Takada, Y., Hishiki, T., Saito, T., Terui, K., Sato, Y., Koseki, H., Yoshida, H., 2009. Induction of Wnt5a-expressing mesenchymal cells adjacent to the cloacal plate is an essential process for its proximodistal elongation and subsequent anorectal development. Pediatr. Res. 66, 149–154.
Padmanabhan, R., 1998. Retinoic acid-induced caudal regression syndrome in the mouse fetus. Reprod. Toxicol. 12, 139–151.
Papapetrou, C., Drummond, F., Reardon, W., Winter, R., Spitz, L., Edwards, Y.H., 1999. A genetic study of the human T gene and its exclusion as a major candidate gene for sacral agenesis with anorectal atresia. J. Med. Genet. 36, 208–213.
Perriton, C.L., Powles, N., Chiang, C., Maconochie, M.K., Cohn, M.J., 2002. Sonic hedgehog signaling from the urethral epithelium controls external genital development. Dev. Biol. 247, 26–46.
Pourquie, O., Coltey, M., Teillet, M.A., Ordahl, C., Le Douarin, N.M., 1993. Control of dorsoventral patterning of somitic derivatives by notochord and floor plate. Proc. Nat. Acad. Sci. U.S.A. 90, 5242–5246.
Rashbass, P., Cooke, L.A., Herrmann, B.G., Beddington, R.S., 1991. A cell autonomous function of Brachyury in T/T embryonic stem cell chimaeras. Nature 353, 348–351.
Renshaw, T.S., 1978. Sacral agenesis. J. Bone Joint Surg. Am. 60, 373–383.
Roelink, H., Augsburger, A., Heemskerk, J., Korzh, V., Norlin, S., Ruiz i Altaba, A., Tanabe, Y., Placzek, M., Edlund, T., Jessell, T.M., et al., 1994. Floor plate and motor neuron induction by vhh-1, a vertebrate homolog of hedgehog expressed by the notochord. Cell 76, 761–775.
Sakai, Y., Meno, C., Fujii, H., Nishino, J., Shiratori, H., Saijoh, Y., Rossant, J., Hamada, H., 2001. The retinoic acid-inactivating enzyme CYP26 is essential for establishing an uneven distribution of retinoic acid along the anterio–posterior axis within the mouse embryo. Gene. Dev. 15, 213–225.
Searle, A.G., 1966. Curtailed, a new dominant T-allele in the house mouse. Genet. Res. 7, 86–95.
Seifert, A.W., Bouldin, C.M., Choi, K.S., Harfe, B.D., Cohn, M.J., 2009. Multiphasic and tissue-specific roles of sonic hedgehog in cloacal septation and external genitalia development. Development 136, 3949–3957.
Showell, C., Binder, O., Conlon, F.L., 2004. T-box genes in early embryogenesis. Dev. Dyn. 229, 201–218.
Siffel, C., Correa, A., Amar, E., Bakker, M.K., Bermejo-Sanchez, E., Bianca, S., Castilla, E.E., Clementi, M., Cocchi, G., Csaky-Szunyogh, M., Feldkamp, M.L., Landau, D., Leoncini, E., Li, Z., Lowry, R.B., Marengo, L.K., Mastroiacovo, P., Morgan, M., Mutchinick, O.M., Pierini, A., Rissmann, A., Ritvanen, A., Scarano, G., Szabova, E., Olney, R.S., 2011. Bladder exstrophy: an epidemiologic study from the International Clearinghouse for Birth Defects Surveillance and Research, and an overview of the literature. Am. J. Med. Genet. C Semin. Med. Genet. 157C, 321–332.
Singh, S.K., Singh, R.D., Sharma, A., 2005. Caudal regression syndrome—case report and review of literature. Pediatr. Surg. Int. 21, 578–581.
Stevenson, R.E., Jones, K.L., Phelan, M.C., Jones, M.C., Barr Jr., M., Clericuzio, C., Harley, R.A., Benirschke, K., 1986. Vascular steal: the pathogenetic mechanism producing sirenomelia and associated defects of the viscera and soft tissues. Pediatrics 78, 451–457.
Stoll, C., Alembik, Y., Dott, B., Roth, M.P., 2007. Associated malformations in patients with anorectal anomalies. Eur. J. Med. Genet. 50, 281–290.
Stott, D., Kispert, A., Herrmann, B.G., 1993. Rescue of the tail defect of Brachyury mice. Gene. Dev. 7, 197–203.
Sulik, K., Dehart, D.B., Iangaki, T., Carson, J.L., Vrablic, T., Gesteland, K., Schoenwolf, G.C., 1994. Morphogenesis of the murine node and notochordal plate. Dev. Dyn. 201, 260–278.
Tam, P.P., Beddington, R.S., 1987. The formation of mesodermal tissues in the mouse embryo during gastrulation and early organogenesis. Development 99, 109–126.
Tam, P.P., Beddington, R.S., 1992. Establishment and organization of germ layers in the gastrulating mouse embryo. Ciba Found. Symp. 165, 27–41, discussion 42-29.
Tam, P.P., Goldman, D., Camus, A., Schoenwolf, G.C., 2000. Early events of somitogenesis in higher vertebrates: allocation of precursor cells during gastrulation and the organization of a meristic pattern in the paraxial mesoderm. Curr. Top. Dev. Biol. 47, 1–32.
Tam, P.P., Tan, S.S., 1992. The somitogenetic potential of cells in the primitive streak and the tail bud of the organogenesis-stage mouse embryo. Development 115, 703–715.
Teillet, M.A., Lapointe, F., Le Douarin, N.M., 1998. The relationships between notochord and floor plate in vertebrate development revisited. Proc. Nat. Acad. Sci. U.S.A. 95, 11733–11738.
Teillet, M.A., Le Douarin, N.M., 1983. Consequences of neural tube and notochord excision on the development of the peripheral nervous system in the chick embryo. Dev. Biol. 98, 192–211.
van de Ven, C., Bialecka, M., Neijts, R., Young, T., Rowland, J.E., Stringer, E.J., Van Rooijen, C., Meijlink, F., Novoa, A., Freund, J.N., Mallo, M., Beck, F., Deschamps, J., 2011. Concerted involvement of Cdx/Hox genes and Wnt signaling in morphogenesis of the caudal neural tube and cloacal derivatives from the posterior growth zone. Development 138, 3451–3462.
van Straaten, H.W., Hekking, J.W., 1991. Development of floor plate, neurons and axonal outgrowth pattern in the early spinal cord of the notochord-deficient chick embryo. Anat. Embryol. (Berl) 184, 55–63.
Vidigal, J.A., Morkel, M., Wittler, L., Brouwer-Lehmitz, A., Grote, P., Macura, K., Herrmann, B.G., 2010. An inducible RNA interference system for the functional dissection of mouse embryogenesis. Nucleic Acids Res. 38, e122.
Watson, E.D., Cross, J.C., 2005. Development of structures and transport functions in the mouse placenta. Physiology (Bethesda) 20, 180–193.
Wilkinson, D.G., Bhatt, S., Herrmann, B.G., 1990. Expression pattern of the mouse T gene and its role in mesoderm formation. Nature 343, 657–659.
Wu, J.I., Centilli, M.A., Vasquez, G., Young, S., Scolnick, J., Durfee, L.A., Spearow, J.L., Schwantz, S.D., Rennebeck, G., Artzt, K., 2007. Tint maps to mouse chromosome 6 and may interact with a notochordal enhancer of Brachyury. Genetics 177, 1151–1161.
Yamaguchi, T.P., Takada, S., Yoshikawa, Y., Wu, N., McMahon, A.P., 1999. T (Brachyury) is a direct target of Wnt3a during paraxial mesoderm specification. Gene. Dev. 13, 3185–3190.
Yanagisawa, K.O., 1990. Does the T gene determine the anteroposterior axis of a mouse embryo? Jpn. J. Genet. 65, 287–297.
Yanagisawa, K.O., Fujimoto, H., Urushihara, H., 1981. Effects of the brachyury (T) mutation on morphogenetic movement in the mouse embryo. Dev. Biol. 87, 242–248.
Ying, Y., Zhao, G.Q., 2001. Cooperation of endoderm-derived BMP2 and extraembryonic ectoderm-derived BMP4 in primordial germ cell generation in the mouse. Dev. Biol. 232, 484–492.
Yoshikawa, Y., Fujimori, T., McMahon, A.P., Takada, S., 1997. Evidence that absence of Wnt-3a signaling promotes neuralization instead of paraxial mesoderm development in the mouse. Dev. Biol. 183, 234–242.